A Section 508–conformant HTML version of this article is available at https://doi.org/10.1289/EHP7030.

Cardiovascular Effects of Polychlorinated Biphenyls and Their Major Metabolites

Fabian A. Grimm,[1] William D. Klaren,[1] Xueshu Li,[2] Hans-Joachim Lehmler,[2] Moumita Karmakar,[3] Larry W. Robertson,[2] Weihsueh A. Chiu,[1] and Ivan Rusyn[1]

[1]Department of Veterinary Integrative Biosciences, College of Veterinary Medicine and Biomedical Sciences, Texas A&M University, College Station, Texas, USA
[2]Department of Occupational and Environmental Health, College of Public Health, The University of Iowa, Iowa City, Iowa, USA
[3]Department of Statistics, College of Science, Texas A&M University, College Station, Texas, USA

Background: Xenobiotic metabolism is complex, and accounting for bioactivation and detoxification processes of chemicals remains among the most challenging aspects for decision making with *in vitro* new approach methods data.

Objectives: Considering the physiological relevance of human organotypic culture models and their utility for high-throughput screening, we hypothesized that multidimensional chemical-biological profiling of chemicals and their major metabolites is a sensible alternative for the toxicological characterization of parent molecules vs. metabolites *in vitro*.

Methods: In this study, we tested 25 polychlorinated biphenyls (PCBs) [PCB 3, 11, 52, 126, 136, and 153 and their relevant metabolites (hydroxylated, methoxylated, sulfated, and quinone)] in concentration–response (10 nM–100 μM) for effects in human induced pluripotent stem cell (iPSC)-derived cardiomyocytes (CMs) and endothelial cells (ECs) (iPSC-derived and HUVECs). Functional phenotypic end points included effects on beating parameters and intracellular Ca^{2+} flux in CMs and inhibition of tubulogenesis in ECs. High-content imaging was used to evaluate cytotoxicity, mitochondrial integrity, and oxidative stress.

Results: Data integration of a total of 19 physicochemical descriptors and 36 *in vitro* phenotypes revealed that chlorination status and metabolite class are strong predictors of the *in vitro* cardiovascular effects of PCBs. Oxidation of PCBs, especially to di-hydroxylated and quinone metabolites, was associated with the most pronounced effects, whereas sulfation and methoxylation of PCBs resulted in diminished bioactivity.

Discussion: Risk characterization analysis showed that although *in vitro* derived effective concentrations exceeded the levels measured in the general population, risks cannot be ruled out due to the potential for population variability in susceptibility and the need to fill data gaps using read-across approaches. This study demonstrated a strategy for how *in vitro* data can be used to characterize human health risks from PCBs and their metabolites. https://doi.org/10.1289/EHP7030

Introduction

Xenobiotic metabolism is a well-recognized modifier of efficacy and toxicity of drugs and chemicals. Extensive characterization of metabolism is required in both drug and chemical safety evaluations (U.S. EPA 2005; U.S. FDA 2017). This process is both time and resource consuming, and data are available on a relatively small number of compounds. For registration of industrial chemicals, there are no requirements for characterization of metabolism; instead, *in silico* models are used to predict both toxicity (Dimitrov et al. 2016) and metabolism (Mekenyan et al. 2012). Limitations of traditional structure–activity models that rely on chemical descriptors to predict biological effects are well recognized (Cronin et al. 2017), especially in distinguishing parent/metabolite pairs, a phenomenon termed "activity cliffs" (Combes 2011). Cell-based assays with appropriate metabolic competence are available for several major tissue types, and they are used in toxicity screening to address the potential adverse effects of metabolites (Rodrigues et al. 2013). Nevertheless, the vast majority of currently available *in vitro* toxicity screening assays lack metabolic competence, and this lack is one key impediment to incorporating new approach methods into hazard and risk assessment (Kavlock et al. 2018).

Polychlorinated biphenyls (PCBs) are one example of a class of compounds with multiple, closely related chemical congeners and toxicologically relevant metabolites (Grimm et al. 2015a). PCBs are persistent organic pollutants with an aromatic biphenyl skeleton containing 1–10 chlorine atoms that comprise a total of 209 congeners (U.S. EPA 2003). PCBs were mass-produced globally between the 1920s and 1990s and used in a variety of industrial and consumer applications (Lauby-Secretan et al. 2013). They are chemically and thermally stable and have accumulated in soil, sediments, and the atmosphere, where they can harm human health and the environment (Lauby-Secretan et al. 2016, 2013). The Stockholm Convention on Persistent Organic Pollutants of 2001, an international treaty that was signed by more than 90 nations, declared prohibition and elimination of production of PCBs and required specific actions to phase out PCBs use over time (Lallas 2001).

Metabolism and disposition of PCBs are complex and depend on the number and positions of chlorine substituents in the molecule (Grimm et al. 2015a; Mathews and Anderson 1975). Therefore, the potential adverse effects of PCB congeners and their metabolites are difficult to ascertain with experiments (Mills et al. 1985); not surprisingly, human health evaluations have been performed on only a relatively small number of these substances and commercial mixtures (Haws et al. 2006; Lauby-Secretan et al. 2013; Silberhorn et al. 1990; Van den Berg et al. 2006). A larger number of congeners and metabolites have been studied *in vitro* (Arulmozhiraja et al. 2005; Kitamura et al. 2005; Ludewig and Robertson 2013), and such an approach may be more feasible for collecting information necessary to establish relative potency of these substances in comparison with that of well-studied PCBs (van Ede et al. 2016). Screening of parent compounds and their metabolites concurrently also addresses the challenge of the lack of metabolism in cell-based assays. Given the higher throughput of *in vitro* assays, metabolites can be queried in concentration–

Address correspondence to Ivan Rusyn, Department of Veterinary Integrative Biosciences, Texas A&M University, College Station, TX 77843 USA. Telephone: (979) 458-9866. Email: irusyn@cvm.tamu.edu

Supplemental Material is available online (https://doi.org/10.1289/EHP7030).

The authors declare they have no actual or potential competing financial interests.

Received 9 March 2020; Revised 6 July 2020; Accepted 6 July 2020; Published 23 July 2020.

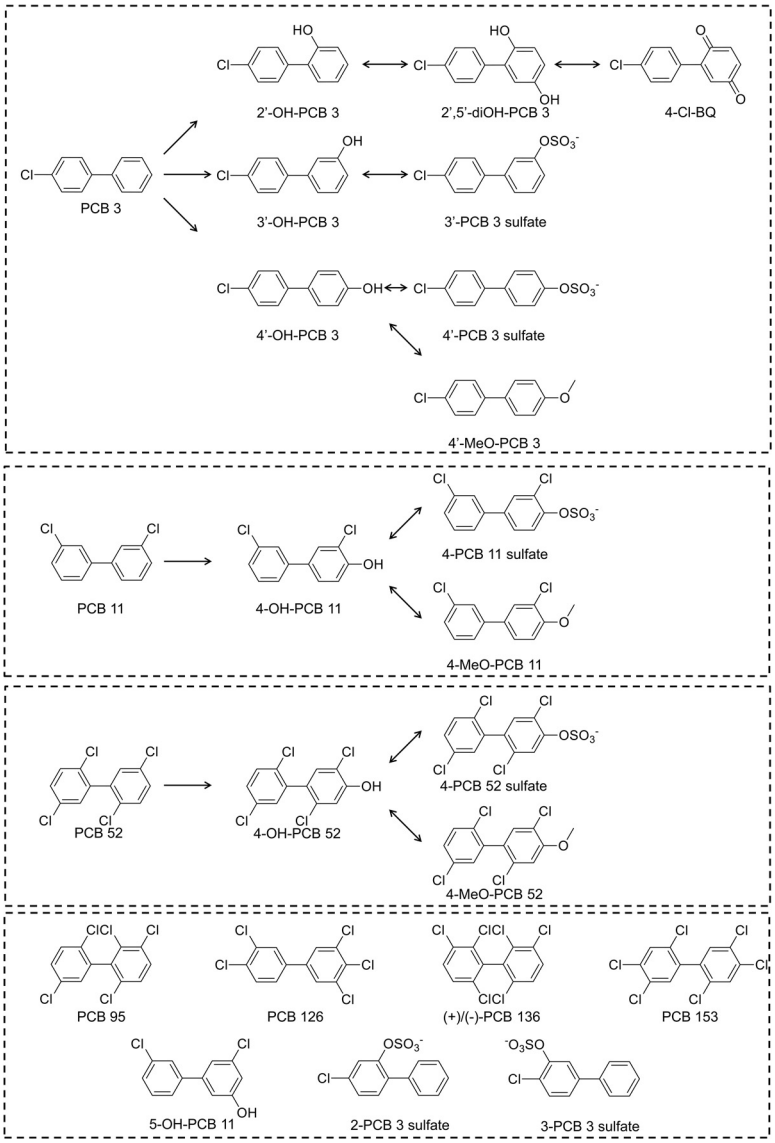

Figure 1. PCBs and their metabolites selected for *in vitro* cardiovascular toxicity testing. The library included three lower chlorinated PCBs (3, 11, and 52) and a selection of hydroxylated, di-hydroxylated, methoxylated, and sulfated metabolites. The higher-chlorinated (≥5 chlorine atoms) PCBs 95, 126, 153, and the atropisomers (+)- and (−)-PCB 136 were also included. Chemical names and abbreviations of PCBs and metabolites are listed in Table S1. Note: PCB, polychlorinated biphenyls.

response for risk-based comparisons with both their rates of metabolism and measured tissue concentrations.

In this study, we conducted comprehensive *in vitro* bioactivity profiling of a diverse selection of environmentally relevant PCBs and, where appropriate, their major metabolites. In addition, we used human exposure data to characterize the margin of exposure (MOE) between *in vitro* concentration–response profiles and serum concentrations of these PCBs and their metabolites in the general population. Exposure assessments demonstrated that many PCBs and metabolites are detectable in humans; however, few of these chemicals have hazard data. To address this deficiency, we used a read-across approach to fill data gaps and enable calculation of cumulative MOEs for each individual in the biomonitoring data sets.

Materials and Methods

Chemical Synthesis and Verification of the Materials

Structures and subclasses of PCBs and their metabolites that were used in this study are shown in Figure 1. PCBs and methoxylated PCBs, including 4-chlorobiphenyl (PCB 3); 2,2′,5,5′-tetrachlorobiphenyl (PCB 52); 2,2′,3,5′,6-pentachlorobiphenyl (PCB 95); 3,3′,4,4′,5-pentachlorobiphenyl (PCB 126); and 2′-methoxy-4-chlorobiphenyl (2′-MeO PCB 3); 3′-methoxy-4-chlorobiphenyl (3′-MeO PCB 3); 4′-methoxy-4-chlorobiphenyl (4′-MeO PCB 3); 4-methoxy-3,3′-dichlorobiphenyl (4-MeO-PCB 11); 5-methoxy-3,3′-dichlorobiphenyl (5-MeO-PCB 11); and 4-methoxy-2,2′,5,5′-tetrachlorobiphenyl (4-MeO-PCB 52) were synthesized using the Suzuki-coupling reaction (Bauer et al. 1995; Joshi et al. 2011; Lehmler and Robertson 2001) following the exact protocol in Lehmler and Robertson (2001). All mono-hydroxylated PCB metabolites of PCB 3, PCB 11, and PCB 52 were obtained by deprotection of the corresponding methoxylated PCB congeners with boron tribromide (Bolgar et al. 1995). 3,3′-Dichlorobiphenyl (PCB 11) was synthesized from 3,3′-dichlorobenzidine by forming a diazonium salt, followed by reduction with hypophosphorous acid (Holland et al. 2017). Symmetrical PCBs, 2,2′,4,4′,5,5′-hexachlorobiphenyl (PCB 153) and racemic 2,2′,3,3′,6,6′-hexachlorobiphenyl (PCB 136), were synthesized using Ullman coupling reaction of the

corresponding chlorinated iodobenzene with copper bronze (Shaikh et al. 2006). PCB sulfates were synthesized by sulfation of hydroxylated PCB congeners with 2,2,2-trichloroethyl chlorosulfate, followed by deprotection with zinc powder/ammonium formate (Li et al. 2010). 2-(4-Chlorophenyl)benzo-2,5-quinone (4-Cl BQ) was prepared via the Meerwein arylation of benzoquinone with 4-chloroaniline (Amaro et al. 1996). 4-Chloro-2′,5′-dihydroxybiphenyl was obtained by reduction of 4-Cl BQ with sodium dithionite (McLean et al. 1996). Atropisomers of PCB 136 were separated on two serially connected 4.6 × 250 mm Nucleodex β-PM columns (Kania-Korwel et al. 2008). The purity of the synthesized PCBs, hydroxylated metabolites, methoxylated derivatives, and the quinone was >99%, as determined by gas chromatography–mass spectrometry (GC-MS). All PCB sulfates were free of decomposition products (i.e., hydroxylated PCBs) according to thin-layer chromatography analysis. See Supporting Information for a description of the synthesis (Table S1 "Chemical names and abbreviations of PCBs and metabolites") and, where applicable, GC-MS authentication (Supplemental Text 1 "Purity determination by GC-MS," and Supplemental Text 2 "Enantiomeric purity determination," and Figures S1–S20 "Gas chromatogram and mass spectra of the individual metabolites") of each PCB derivative used in this study. For general information regarding purity determinations, see Li et al. (2018).

Chemical and Biological Materials

iCell® cardiomyocytes (Cat. No. CMC-100-010-001) and respective plating and maintenance media, iCell® endothelial cells (Cat. No. ECC-100-010-001) and their requisite media supplements were purchased from FujiFilm Cellular Dynamics International. Trypan blue solution (0.4%) and penicillin/streptomycin (50 mg/ml) were obtained from Life Technologies. Dimethyl sulfoxide (DMSO, tissue culture grade) was purchased from Santa Cruz Biotechnology. Chloroquine phosphate, nocodazole, suramin, and tetraoctyl ammonium bromide (TAB) were from Cayman Chemical. Isoproterenol and propranolol were purchased from Molecular Devices, and cisapride was obtained from Sigma Aldrich. VascuLife® containing Vascular Endothelial Growth Factor (VEGF) Medium Complete Kits recommended for iCell®-endothelial cells culture were purchased from Lifeline Cell Technology. Pooled HUVECs in EGM-2 media (Cat. No. CC2519A) and EGM™-2 BulletKits™ were obtained from Lonza. Biological reagents and cellular dyes, including Calcein AM, fibronectin, Geltrex™ LDEV-Free reduced growth factor basement membrane, Hoechst 33342, and TrypLE™ Express were procured from Life Technologies. Media, supplements, and positive controls, including fetal bovine serum, histamine, FluoroBright Dulbecco's Modified Eagle's Medium (DMEM), and Medium 199 were purchased from Fisher Scientific.

Calculation of the Physicochemical Descriptors

Physicochemical descriptors (molecular weight, logP, logS, density, polarizability, molar volume, surface tension, and percent composition based on carbon, hydrogen, chlorine, oxygen, and sulfur content) were all calculated in ChemSketch (ACD/Labs). Numbers of ortho-, meta-, and parachlorines, total number of chlorines, and number of ortho-, meta-, and para-(nonchlorine)alkyl groups (e.g., hydroxyl- or sulfooxy-) were based on manual counts.

Cell Culture

Details on cardiomyocyte cell culture are described in detail elsewhere (Grimm et al. 2015b; Sirenko et al. 2013a). Briefly, tissue-culture treated 384 well plates were gelatinized with 25 μL per well of 0.1% (w/v) gelatin in water for 2 h at 37°C and 5% CO_2. Individual vials of cells were thawed for 4 min in a water bath maintained at 37°C. Thawed cells were resuspended in 10 ml plating medium containing 1:500 (vol/vol) penicillin/streptomycin solution at room temperature (RT). Live cell counts for each cell suspension were determined by trypan blue staining and cells were further diluted to provide final cell densities of 2×10^5 viable cells/ml. Thus, 5,000 cells suspended in 25 μL media were transferred per well after the gelatin solution had been discarded. Cell culture plates were rested for 30 min at RT before they were incubated for 48 h at 37°C and 5% CO_2. Then, a media exchange with 30 μL of fresh maintenance medium containing 1:500 (vol/vol) penicillin/streptomycin solution was performed, and cell media were subsequently changed every 48 h for 12 d. On the experiment day, the medium was completely exchanged with either 25 μL (for Ca^{2+} flux assay) or 40 μL (for imaging) of fresh medium.

The culture conditions of iCell®-endothelial cells were as reported elsewhere (Iwata et al. 2017). Briefly, T75 flasks were coated with a fibronectin solution (3 $\mu g/cm^2$) followed by incubation for 1–2 h. Cells were thawed for 3 min in a 37°C water bath. Thawed cells were added to maintenance medium made of VascuLife VEGF Medium Complete Kit, excluding the supplied FBS, and iCell® Endothelial Cells Medium Supplement. The final formulation of the maintenance medium is detailed in (Iwata et al. 2017). The aliquoted fibronectin solution was aspirated from the T75 flasks, and cells were seeded at 1.0×10^4 cells/cm^2. Cells were maintained at 37°C and 5% CO_2 with media changes occurring every 2 d and passaged every 3–4 d using TrypLE™ Express. All experiments were conducted on cells between passages 1 and 5.

Similar to the cultivation of iCell®-endothelial cells, HUVEC maintenance and experimentation are detailed elsewhere (Iwata et al. 2017). Briefly, HUVECs were thawed, seeded, and grown in T75 tissue culture flasks in Medium 199 with EGM™-2 BulletKits™. HUVECs were incubated at regular cell culture conditions, 37°C and 5% CO_2, and passaged every 2–3 d using TrypLE™ Express. To ensure adequate endothelial function, experiments were performed with cells between passages 1 and 5.

Evaluation of the Effects on the Function of CMs

Responses of iCell®-cardiomyocytes to drugs and chemicals were evaluated using intracellular Ca^{2+} flux measurements (Grimm et al. 2015b; Sirenko et al. 2013b). For experiments, 20 mM stock solutions of PCBs and PCB metabolites were prepared in DMSO (200×). Chemical working solutions (5×) were prepared using cardiomyocyte maintenance medium and contained 2.5% (vol/vol) DMSO. These chemical master plates were prepared to include all chemicals in concentration–response (0.05, 0.5, 5, 50, and 500 μM). Negative controls included media-only and vehicle control (i.e., 0.5% vol/vol DMSO in cell culture media) wells. Positive assay controls were consistent with previously published reports (Grimm et al. 2018) and included TAB (50 μM) as a cytotoxic control, and isoproterenol (0.1–10 μM), propranolol (0.1–5 μM), cisapride (0.01–1 μM), and doxorubicin (0.1–5 μM) as chemicals associated with specific effects on beating and ion flux. Each test chemical was screened in triplicate for each concentration.

Experiments started with the addition of 25 μL of prewarmed 2× concentrated calcium dye reagent to sample wells containing 25 μL maintenance media. Microplates were then acclimated for 2 h at 37°C. Following equilibration, cardiomyocyte sample wells were treated simultaneously by the addition of 12.5 μL of prewarmed 5× chemical solution to iCell®-cardiomyocytes using the automated liquid handler in the FLIPR tetra (Molecular Devices). Treated cell cultures were incubated for either 90 min or 24 h. After the conclusion of the treatment period, the Ca^{2+} flux was measured for 100 s at a frequency of 8 Hz using the integrated fluorescence plate reader in the FLIPR tetra (Molecular Devices) using an emission wavelength range of $\lambda_{emission} = 515–575$ nm ($\lambda_{excitation} = 470–495$ nm). Additional instrument settings included

exposure time per read of 0.05s, a gain of 2000, an excitation intensity of 30%, and an internal temperature of 37°C.

Ca^{2+} flux data were processed in R studio (version 1.0.136, with R version 3.3.2; R Development Core Team) as described elsewhere (Blanchette et al. 2019; Burnett et al. 2019). Calculated quantitative metrics included the means and coefficients of variation (CV) of the peak height, which can be indicative of cytotoxicity, inhibition, or stimulation of beating. Means of peak frequency, an indicator of positive or negative inotropes, and CV of peak spacing, an indicator of irregular beating, were also derived from Ca^{2+} flux traces. Finally, the mean ratio of the decay over rise time was calculated. Increases in the decay/rise time ratio are reflective of delayed repolarization and are a measure for QT prolongation.

Evaluation of Cardiotoxic Effects

Cytotoxicity and effects on mitochondrial integrity of various PCBs and PCB metabolites in induced pluripotent stem cell-CMs (iPSC-CMs) were assessed using high-content cellular imaging in ImageXpress® Micro Confocal (Molecular Devices) as detailed in (Grimm et al. 2015b). Cells in 40 μL maintenance media were treated with 10 μL of 5× chemical solutions to provide test chemicals at final assay concentrations ranging from 0.01 to 100 μM. Following the addition of chemicals, cells were incubated at 37°C and 5% CO_2 for 24 h. Next, sample wells were treated with 50 μL equilibrated 2× concentrated staining solution (maintenance medium containing Hoechst 33342, 4 μg/mL and MitoTracker™ Orange, 0.4 μM). Microplates were then incubated for 15 min at 37°C and 5% CO_2 before cells were washed twice with 30 μL maintenance medium. All media were aspirated and discarded, and cells were fixed with 25 μM of a 3.7% formaldehyde solution for 15 min at 37°C and 5% CO_3. Fixed cells were washed 3× with 25 μL PBS before image acquisition using the DAPI (Hoechst 33342) and Cy3 (MitoTracker™ Orange) filters at 10× magnification on the ImageXpress® Micro Confocal high-content confocal microscope (Molecular Devices). The multiwavelength cell scoring applications module in MetaXpress® was used to analyze acquired images.

Evaluation of the Effects on ECs

Tube formation assays were performed on Geltrex™ LDEV-free reduced growth factor basement membrane using both iCell®-endothelial cells and HUVECs in 384-well format exactly as detailed in Iwata et al. (2017). Negative controls included media-only and vehicle control (i.e., 0.5% vol/vol DMSO in cell culture media) wells. Positive assay controls were consistent with previously published reports (Iwata et al. 2017) and included TAB (50 μM) as a cytotoxic control, and nocodazole (0.01–1 μM), suramin (0.5–50 μM), histamine (0.1–100 μM), and chloroquine (1–500 μM) as chemicals associated with specific effects on ECs. Each test chemical was screened in triplicate for each concentration. Briefly, for iCell®-endothelial cells, starvation media consisted of VascuLife® basal medium with 4 mM L-glutamine LifeFactor and 0.1% iCell®-endothelial cells medium supplement. To counter dilution effects, a 2× concentration of the HUVEC maintenance medium supplemented with additional VEGF was created (EGM™-2 BulletKits™ at 2× concentration; also the VEGF component was replaced with 12.5 ng/mL VEGF). Geltrex™ LDEV-free reduced growth factor basement membrane was thawed overnight and dispensed into 384-well plates (10 μL/well) with tapping and rotating to evenly coat. The plates were incubated for 1 h in a cell culture incubator at 37°C and 5% CO_2. A 2× PCB plate (containing all of the PCBs and metabolites in dose–response) was prepared in basal media and added, 25 μL per well, to the Geltrex™ coated plates. On separate plates, cells were seeded 7,500 (iPSC- ECs) or 3,500 (HUVEC) cells/well. Cells were exposed to chemicals overnight at 37°C and 5% CO_2 and stained with 3× concentration of calcein AM (25 μL/well, 6 μmol/L) for 15 min before imaging. Images were captured at 4× magnification with the FITC filter (calcein AM). Images were analyzed with the angiogenesis module software within MetaXpress™ (Molecular Devices).

Cytotoxicity was assessed in parallel experiments. For iCell®-endothelial cells, 384-well plates were coated with a 30 μg/mL fibronectin solution (10 μL/well) and incubated for 2 h at RT. iCell®-endothelial cells were dissociated with TrypLE™ Express and prepared into a solution to achieve 750 cells per well and 50 μL of total volume. The fibronectin solution was removed from the 384-well plate, and cells were plated. For HUVECs, similar dissociation and the same cell density were used for plating with the exclusion of the fibronectin solution. Cells were incubated at 37°C and 5% CO_2 until a monolayer was formed, typically 3–5 d. 2× PCB plates were created with the requisite maintenance medium. Before treatment, the medium in the wells was exchanged to 25 μL/well of fresh maintenance medium. 2× PCB chemical solutions (12.5 μL/well) were added. After 24 h incubation at 37°C and 5% CO_2, cells were stained with Hoechst 33342, MitoTracker™ Orange, and calcein AM for 20 min before replacing the staining media with FluoroBright DMEM. Cell culture plates were imaged using the ImageXpress® Micro Confocal high-content imaging system (Molecular Devices). Images were acquired at 10× magnification with DAPI, TRITC, or FITC filter (Hoechst 33342, MitoTracker™, or calcein AM, respectively). The multiwavelength cell scoring applications module in MetaXpress™ (Molecular Devices) was used to analyze the images.

Data Analysis and Visualizations

Phenotypic responses were quantitatively assessed using concentration–response modeling as detailed elsewhere (Sirenko et al. 2017). Briefly, phenotypic readouts were normalized to vehicle controls and fit to a four-parameter logistic model in R studio software (version 3.1.1; R Development Core Team). Following EPA guidance on dose–response modeling, a cutoff of one standard deviation across means of vehicle control (i.e., 0.5% vol/vol DMSO in cell culture media) wells was applied to determine the point-of-departure (POD) values (U.S. EPA 2012). In the absence of a concentration–response, the highest tested concentration (i.e., 100 μM) was assigned as "no observable adverse effect level." The concentration–response assessment R script, as well as templates for vehicle and concentration–response data, are available as a supplement to Sirenko et al. (2017). The ability of physicochemical properties to predict differences in PODs were evaluated by multiregression and mixed-effects modeling using R.

POD values were then integrated using ToxPi 2.0 (Marvel et al. 2018) software. In ToxPi, each slice is representative of cell type– and time-point–specific phenotypes. The area of each slice is proportional to the relative value (e.g., bioactivity or physicochemical descriptor value) of the chemical within the data set. ToxPi scores were used to rank PCBs and their metabolites according to their overall bioactivity and to determine variability in total observable biological responses and chemical characteristics for each major metabolite class and chlorination status (mono-, hexa-chlorinated). Additional visualizations such as dumbbell and principal components analysis plots were generated in R Studio (version 1.1.456; R version 3.5.1; R Development Core Team) using the ggplot2 package.

Risk Characterization Based on the Margin of Exposure

Characterization of the margins of exposure for PCBs and their metabolites was achieved by cell type–specific comparison of measured bioactivity, i.e., calculated POD values, and human

serum concentrations of selected PCBs, hydroxylated metabolites of PCBs (OHPCBs), and PCB sulfates. PCB and OHPCB serum concentrations were based on the data from the Airborne Exposure to Semi-Volatile Organic Pollutants study (Ampleman et al. 2015; Grimm et al. 2017; Koh et al. 2016a, 2016b).

As an initial screen, the cell type– and PCB/metabolite–specific PODs were compared with the range of total exposures across each class (PCBs, OHPCBs, and PCB sulfates). Specifically, for each class, the ranges were derived for total (parent) PCB content in serum samples from 175 individuals, total OHPCB content in serum samples from 159 individuals, and 4-PCB 11 sulfate in 46 individuals. For each class, ranges (min–max were compared with distributions of biological activity per congener (individual PCB, OHPCB, or PCB sulfate) and cell type (i.e., iCell® cardiomyocytes, iCell®-endothelial cells, and HUVECs), represented by box plots. Reported values in nanograms of PCB or OHPCB per gram of fresh serum weight were converted to their approximate molar concentrations based on an average serum density of 1.025 g/mL and an approximate PCB or OHPCB molecular weight of 300 g/mol.

The initial screening analysis compared total class concentrations with individual congener or metabolite bioactivity and does not take into account within-class variation in potency or cumulative risks from across all congeners and classes. To address these issues, as well as to characterize population variability, a cell-type–specific, cumulative margin of exposure was calculated for each individual within the sampled population (van der Voet et al. 2009). Because there are missing data in both the exposure and bioactivity datasets, both "central tendency" and "conservative" imputation/read-across approaches were used to fill data gaps. For exposure, missing data were imputed using either the median ("central tendency") or 95th percentile ("conservative") across the individuals with data for that particular congener or metabolite (nondetects were treated as zero but included in the calculation). For bioactivity, for each chemical- and cell-type, the fifth percentile POD was assigned as the "critical" end point to be used for MOE calculations, following the approach used by Paul Friedman et al. (2020). Then, for chemicals without data, a class-based read-across for each cell type was used, whereby missing PODs were replaced either using the median ("central tendency") or minimum ("conservative") across members of the same class, a common approach for read-across. Then, for each cell type and individual, the cumulative MOE was derived by taking the harmonic sum of the compound-specific MOEs (van der Voet et al. 2009). The resulting distribution of individual MOEs for each cell type was characterized using box plots, with "central tendency" and "conservative" imputation/read-across approaches compared.

Results

Testing of the Effects of PCBs and Metabolites in Human CMs and ECs

A total of 25 PCBs and their metabolites (Figure 1) were tested in concentration–response (0.01–100 μM) using human iPSC-CMs and ECs, and HUVECs. Figure 2A shows representative Ca^{2+} flux traces in experiments with human iPSC-CM for media, vehicle, or three selected PCB metabolites, 4′-MeO-PCB 3, 5-OH-PCB 11, and 4-OH-PCB 52. A positive inotropic effect, i.e., an increase in the beat rate, was observed after treatment with 100 μM of 4′-MeO-PCB 3. Treatment with 100 μM of 5-OH-PCB 11 or 4-OH-PCB 52 resulted in a complete block of Ca^{2+} flux because of the loss of cell viability at this concentration (Figure 2A). Representative images of the effects on the tubular networks in human iPSC-derived ECs are shown in Figure 2B. Increases in the density and number of formed "tubes" were observable for some of the PCB metabolites at lower concentrations (i.e., 0.01 μM, as exemplified by all three chemicals shown), but at higher concentrations (above 1 μM, as exemplified by all three chemicals shown), the networks were disrupted (See Figure 3 and Supplemental Excel file for details on the effects of each tested compound).

Quantitative concentration–response profiles for all tested PCBs and metabolites in all three cell types are shown as heat maps in Figure 3. Effects on cytotoxicity end points and those on the end points representative of the physiological function of each cell type are shown separately. For iPSC-CMs, the 100 μM concentration of almost all compounds was cytotoxic at both 90 min (Figure 3A) and 24 h (Figure 3B) of exposure. Many compounds exhibited effects on cell beating parameters at noncytotoxic concentrations at both time points. Chemical structure-dependent trends in effects were evident, with low-chlorinated PCB 3 and PCB 11 sulfates, 4′MeO-PCB 3, and PCB 126 having little effect on cell viability. PCB 126, PCB 3, and its methoxylated metabolite 4′-MeO-PCB 3 were found to have positive inotropic effects. Cytotoxic and other effects were highly concordant between 2′,5′-diOH-PCB 3 and 4-Cl-BQ.

Concentration-responses for *in vitro* tubulogenesis and cytotoxicity in iPSC-EC and HUVEC are shown in Figures 3C–D. Concordant with observations in iPSC-CMs, cell viability was affected by most compounds at the highest tested concentration. In

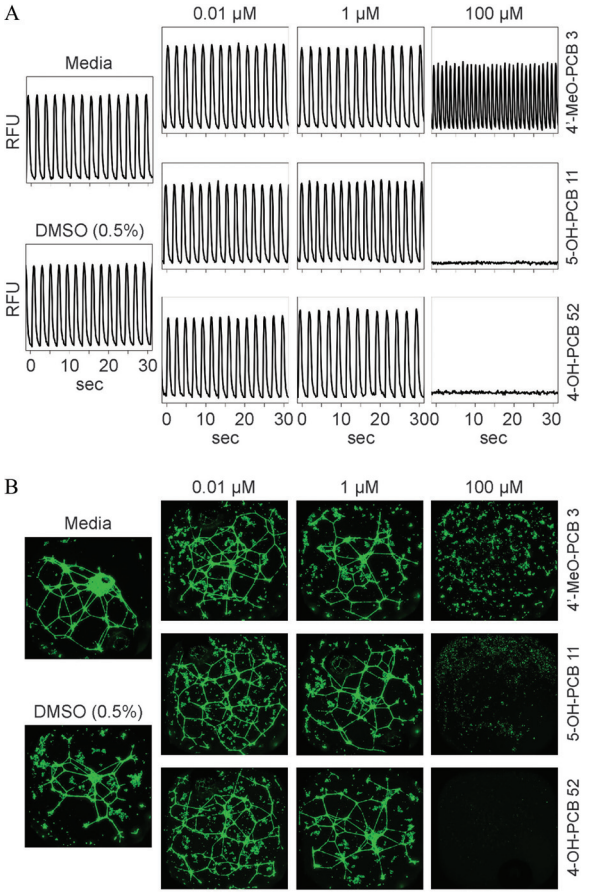

Figure 2. Effects of PCB metabolites on iCell®-cardiomyocytes and iCell®-endothelial cell. (A) Representative Ca^{2+} flux traces (90 min after treatment) for media, vehicle (0.5% DMSO) or three PCB metabolites at three concentrations on iPSC-derived CMs. (B) Representative images of the tubular networks for media, vehicle (0.5% DMSO), or three representative PCB metabolites at three concentrations on iPSC-derived ECs. Images were acquired at 4× resolution. Chemical names and abbreviations of PCBs and metabolites are listed in Table S1. Note: CMs, cardiomyocytes; DMSO, dimethyl sulfoxide; ECs, endothelial cells; iPSC, induced pluripotent stem cell; PCBs, polychlorinated biphenyls.

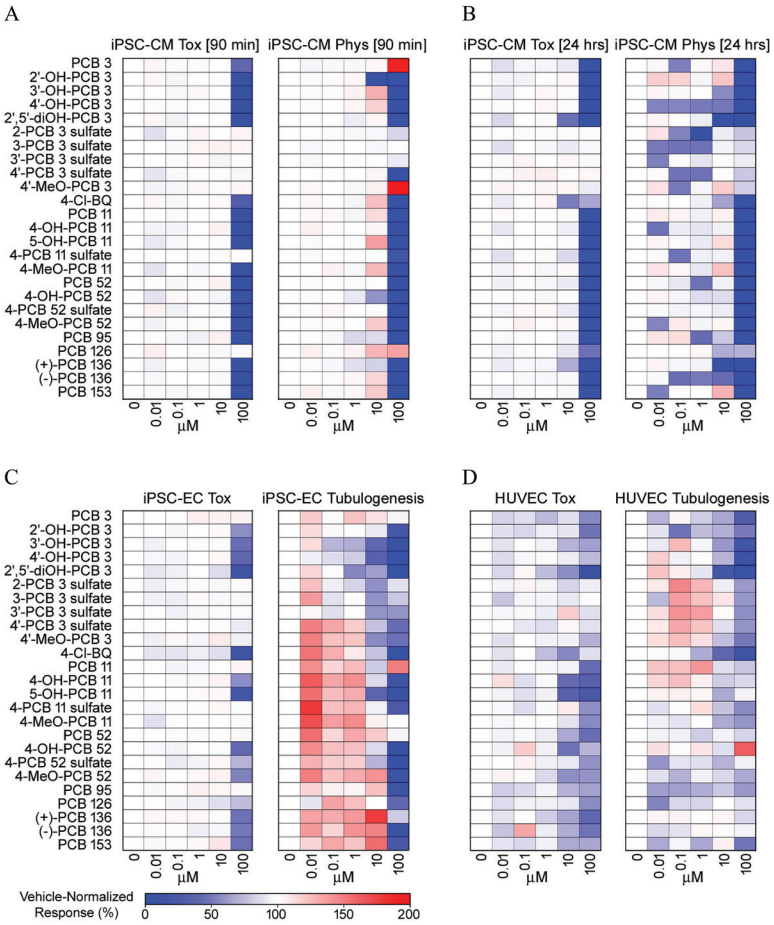

Figure 3. Heatmaps of concentration-related effects of PCBs and their metabolites in different cell types and time points. (A) Effects in iPSC-CMs at 90 min after exposure ("Tox" is cell viability and "Phys" is beats per minute phenotypes). (B) Effects in iPSC-CMs at 24 h after exposure ("Tox" is cell viability and "Phys" is beats per minute phenotypes). (C) Effects in iPSC-ECs ("Tox" is cell viability at 24 h, and "Tubulogenesis" is total tube length at 18 h phenotype). (D) Effects in HUVECs ("Tox" is cell viability at 24 h, and "Tubulogenesis" is total tube length at 18 h phenotype). The effects at each concentration were normalized to respective vehicle controls (i.e., 100%, white color). Relative increases and decreases in the respective assay signal are shown as red and blue gradients. Chemical names and abbreviations of PCBs and metabolites are listed in Table S1. Data for each cell and phenotype are available in the Supplemental Excel file, tabs iPSC-CMs; iPSC-ECs; HUVECs. Note: CMs, cardiomyocytes; ECs, endothelial cells; HUVECs, human umbilical vein endothelial cells; iPSC, induced pluripotent stem cell; iPSC-CMs, iPSC-derived cardiomyocytes; iPSC-ECs, iPSC-derived endothelial cells; PCBs, polychlorinated biphenyls; ToxPi, Toxicological Prioritization Index.

iPSC-ECs, there was a clear trend for cytotoxicity of lower-chlorinated congeners and mono- and di-hydroxylated metabolites. On the contrary, parent PCBs 3 and 11, as well as their sulfated and methoxylated metabolites, did not affect cell viability. iPSC-EC tubulogenesis assay showed that PCBs and metabolites could increase tube formation even at the lowest test concentration (10 nM). Mono- and di-hydroxylated PCB 3 metabolites were among the most potent inhibitors of iPSC-EC tubulogenesis, a finding that was concordant with their cytotoxicity. The effects of test chemicals on iPSC-EC and HUVEC viability were mostly concordant, even though HUVECs were more sensitive than iPSC-ECs. Concordant effects included cytotoxicity at the highest tested concentrations and identified mono- and di-hydroxylated PCB metabolites as the most cytotoxic. In addition, concentration–responses of the structural analogs, including (+)- and (−)-PCB 136, 4-OH-PCB 11 and 5-OH-PCB 11, and 2′,5′-di-OH-PCB 3 and 4-Cl-BQ, were also highly consistent between both cell types.

Structure–Activity Relationships in the Effects of PCBs and Metabolites in Human CMs and ECs

Structure-activity relationships for PCB congeners are well established, based on animal studies *in vivo* and understanding of the metabolism of these compounds (Safe 1993; Van den Berg et al. 2006). Therefore, we used data from human CMs and ECs, as well as physicochemical properties of the test chemicals, to examine structure–activity trends in their *in vitro* effects. Multiregression and mixed-effects models using physicochemical properties were unable to model individual PODs, in part due to the relatively large number of phenotypes and the small number of independent variables (not shown). Therefore, data visualization and clustering were performed using the ToxPi 2.0 software tool (Marvel et al. 2018) that allowed integration and aggregation of complex data sets using normalized scores and pie chart images.

Three analyses were performed (Figure 4A): *in vitro* "bioactivity" data alone, physicochemical properties alone, or a combination of the two, the so-called chemical-biological analysis (Low et al. 2013). For *in vitro* data (Figure 4B), POD values were obtained for each phenotype and data were aggregated by cell type, time point, and type of response (cytotoxicity vs. physiological phenotypes). We found that *in vitro* data demonstrated good concordance between the biological activity of closely related PCBs and metabolites. For example, 2′,5′-diOH-PCB 3 and 4-Cl-BQ, the atropisomers (+)- and (−)-PCB 136, the sulfates of PCB 3, and mono-hydroxylated forms of PCB 3 were clustered together. Clustering analysis based on physicochemical descriptors resulted in an even

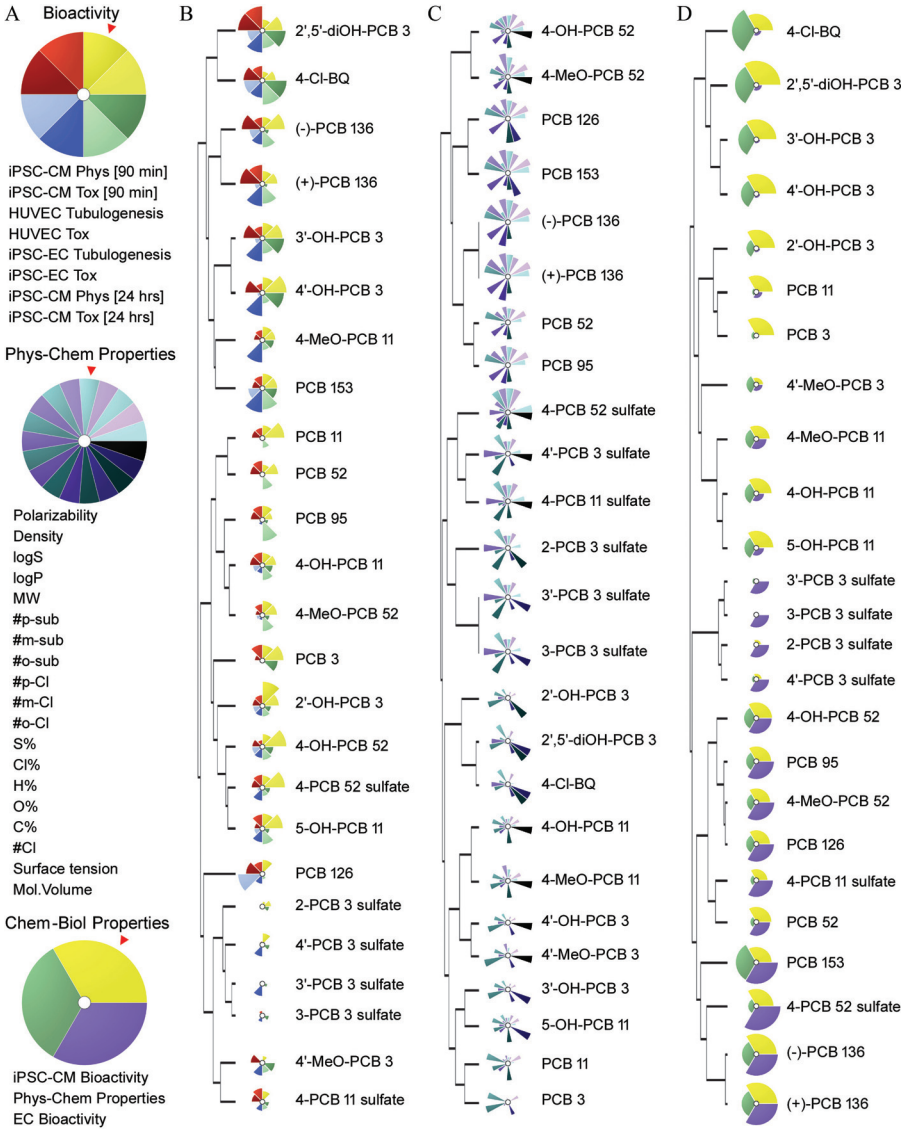

Figure 4. Clustering analysis of PCBs and their metabolites using the ToxPi. (A) Color diagram for data integration into pie chart slices for each type of analysis (*in vitro* toxicity data, physicochemical properties, and combination of the two). (B) Clustering using *in vitro* data where point-of-departures values derived from 30 phenotypic assays were grouped into eight categories (iPSC-CMs' physiological responses and cellular toxicity after 90 min and 24 h, and iPSC-ECs' and HUVECs' tubulogenesis and cellular toxicity data). A summary of point-of departure values is shown in the Supplemental Excel file, tab POD summary. (C) Calculated physicochemical descriptors were used for the generation of ToxPi and clustering. (D) Clustering based on a combination of in vitro and physicochemical data. In ToxPi images, each slice is a representation of cell type- and time-point-specific phenotypes or scaled values associated with a physicochemical characteristic, the area of each slice is proportional to the relative value of the effect for a given chemical within the dataset. Each ToxPi is corresponding to one compound tested in this study. Chemical names and abbreviations of PCBs and metabolites are listed in Table S1. Data for each ToxPi are available in the Supplemental Excel file, tab ToxPi_summary. Note: CMs, cardiomyocytes; ECs, endothelial cells; HUVECs, human umbilical vein endothelial cells; iPSC, induced pluripotent stem cell; iPSC-CMs, iPSC cardiomyocytes; PCBs, polychlorinated biphenyls; ToxPi, Toxicological Prioritization Index.

more pronounced clustering of structurally related PCBs and metabolites (Figure 4C). Physicochemical descriptors and biological activity data were then combined into three equally weighted slices: iPSC cardiomyocyte phenotypes, EC phenotypes, and physicochemical descriptors (Figure 4D). Major trends observable with the individual data streams were preserved in the integrated analysis, i.e., structural similarity appeared to be closely related to the biological activity. The highest similarity was observed for quinoid species, hydroxylated PCB 3 metabolites, sulfated PCB 3 metabolites, and PCB 136 atropisomers. Interestingly, different metabolites of a given PCB congener (i.e., PCB 3) clustered together, indicating that the chlorine-substitution status and pattern were key determinants of the *in vitro* effects of PCBs and their metabolites.

To further examine structure–activity trends in the activity of parent PCBs and their metabolites, we conducted a quantitative analysis of the ToxPi scores from the analyses shown in Figure 4. Clear trends associating biological activity with PCB chlorination pattern and metabolite class are evident (Figure 5). *In vitro* effects on CMs and ECs were weakly dependent on the number of chlorine substituents; however, metabolite class was a much stronger predictor of the *in vitro* effects (Figure 5A). PCB sulfates were least bioactive, followed by methoxylated PCB metabolites and parent PCBs. Oxidative metabolism of PCBs to mono- and di-hydroxylated, and quinone species was associated with incremental increases in the *in vitro* effects; di-hydroxylated and quinone metabolites were most potent. Physicochemical descriptors ranked test compounds by the

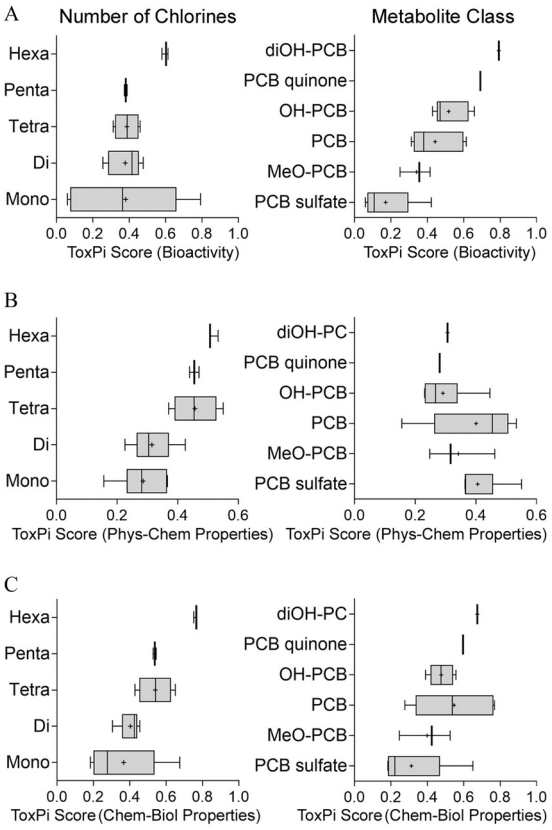

Figure 5. Ranking of the PCBs and their metabolites chemical classes using (A) *in vitro* testing data, (B) physicochemical descriptors, or (C) combination of the two. Groupings based on the number of chlorine atoms (left panels) or metabolite class (right panel) are shown. ToxPi scores from the analysis shown in Figure 4 were used to generate box-and-whisker plots for each group. Individual box-and-whisker plots indicate the median (line), mean (cross), interquartile range (box), and min–max span (whiskers). Chemical names and abbreviations of PCBs and metabolites are listed in Table S1. Note: PCB, polychlorinated biphenyls; ToxPi, Toxicological Prioritization Index.

chlorination status, but not by the metabolite class (Figure 5B). When both *in vitro* data and physicochemical properties were combined, clear trends were observed in both directions—the number of chlorines and metabolite class (Figure 5C).

We also sought to examine metabolism-associated trends in the *in vitro* effects at the individual congener level (Figure 6). Biological activity was primarily determined by metabolic status (Figure 6A) but also affected by the chlorination pattern. For lower-chlorinated PCBs 3 and 11, sulfation resulted in an overall decrease in bioactivity, whereas oxidation increased bioactivity compared to the parent congener. However, for the tetra-chlorinated PCB 52, sulfation increased the parent PCB-associated bioactivity. Chlorination appeared to be less of a predictor of bioactivity among lower-chlorinated congeners, i.e., PCB 3, 11, and 52, but seemed to be associated with increases in biological activity for congeners containing five or more chlorine substituents. ToxPi scores based on physicochemical descriptors showed an increased value for the metabolites in comparison with the respective parent, and chlorination was a distinguishable feature among selected chemicals (Figure 6B). Combining both biological and chemical properties in ToxPi 2.0 resulted in both chemical characteristic (i.e., chlorination pattern) and biological activity (i.e., metabolite status) determined ranking, with increases in chlorination and oxidation being associated with increased biological activity (Figure 6C). Across all analyses (biological, chemical, and chemical-biological) PCBs and PCB metabolites with clearly distinguishable structural features clustered well together. Examples for structurally related clusters included PCB sulfates, diOH-PCB 3 and 4-Cl-BQ, and MeO-PCBs.

Risk Characterization for Human Cardiovascular Effects Based on in Vitro *Data*

To facilitate the interpretation of the observed *in vitro* effects in a risk assessment context, margins of exposure were determined for each of the assessed PCBs and metabolites (Figure 7). We used human exposure data, where available (Ampleman et al. 2015; Grimm et al. 2017; Koh et al. 2016a, 2016b), to estimate serum concentration ranges for exposed subjects. As an initial risk characterization approach, POD values for each cell type were combined into one box-and-whiskers plot per chemical tested, plotted as nominal *in vitro* concentrations, and compared with the ranges of total human serum-free fractions, shown separately for parent PCBs (Figure 7A) and their hydroxylated (Figure 7B) or sulfated (Figure 7C) metabolites. For the parent PCBs, the lower chlorinated congeners (PCB 3, 11, and 52) had two to three orders of magnitude margin between the lowest effect level *in vitro* and highest measured human serum concentrations (Figure 7A). For higher chlorinated PCBs and effects in some cell types, the margins were less than two orders of magnitude or were overlapping (i.e., for PCB 95 in HUVECs and PCB 153 in iCell®-endothelial cell). For hydroxylated PCBs, the margins varied from over three orders of magnitude to less than one (Figure 7B). For the sulfated PCBs, even though human biomonitoring data suggested that their serum concentrations were generally higher than those of parent molecules or hydroxylated metabolites (Ampleman et al. 2015; Grimm et al. 2017; Koh et al. 2016a, 2016b), MOEs were generally over one order of magnitude (Figure 7C).

However, our initial risk characterization analysis did not take into account within-class variation in potency or cumulative risks from across all congeners and classes, nor did it take into account the likelihood of population variability in exposures. Addressing cumulative risks is hampered by the large number of PCBs and metabolites measured in comparison with the small number of PCB derivatives for which bioactivity data are available. Thus, as a follow-up analysis, we used an imputation/read-across approach to fill data gaps and enable calculation of cumulative MOEs for each individual in the biomonitoring data set. Both a "central tendency" approach and a "conservative" approach were taken, with the results shown in Figure 7D. The "central tendency" approach yielded cumulative MOEs at or above 100 for most individuals, with a few individuals with MOEs around 10. However, the "conservative" approach resulted in MOEs around 10 for ECs and HUVECs, with higher MOEs around 100 for CMs. One individual had MOEs <1 for both ECs and HUVECs.

Discussion

In this study, we aimed to compare the *in vitro* effects of a diverse compendium of PCBs and their major metabolites representing major congeners of interest from a public health perspective (Grimm et al. 2015a). In addition, tested compounds represented the broad range of structural variability of PCBs, including the degree of chlorination and substitution pattern, and biotransformation-associated metabolites. The test library included three lower-chlorinated, (semi) volatile PCB congeners, PCBs 3 (mono-chlorinated), 11 (di-chlorinated), and 52 (tetra-chlorinated). These lower-chlorinated congeners gained attention primarily through their detectability in air samples in schools, a result of their emission from building materials (Herrick et al. 2016; Marek et al. 2017). In addition, PCB 11 was identified as a nonlegacy PCB, and its

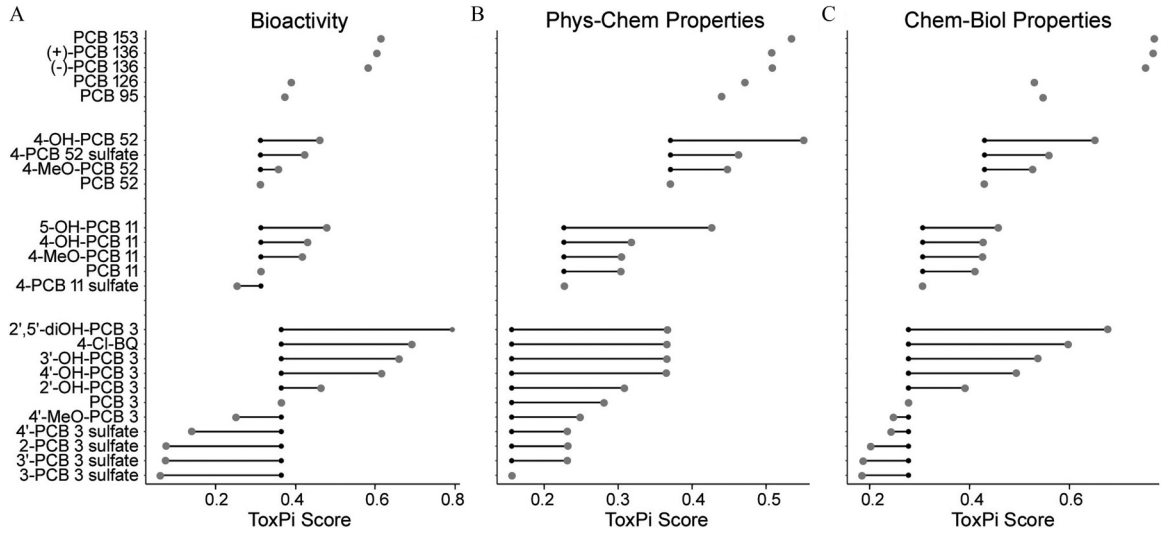

Figure 6. Relative change in the *in vitro* potency of the parent PCBs, depending on (A) their metabolism, and (B) integrated congener- and metabolite-specific distributions of calculated physicochemical characteristics, and (C) integrated chemical-biological profiles. ToxPi scores for each compound are plotted based on the analysis in Figure 4. Chemical names and abbreviations of PCBs and metabolites are listed in Table S1. Small black dots are ToxPi scores for the respective parent PCB congener; large gray dots are ToxPi scores for PCB metabolites; connecting lines indicate PCB parent–metabolite relationship. Data on ToxPi scores are provided in the Supplemental Excel file, tab ToxPi Scores. Note: PCBs, polychlorinated biphenyls; ToxPi, Toxicological Prioritization Index.

continued environmental release has been associated with paint and pigment manufacturing (Hu and Hornbuckle 2010). Both parent PCB 11 and its hydroxylated, glucuronidated, and sulfated metabolites have been detected in blood samples of exposed individuals (Grimm et al. 2017; Sethi et al. 2017, 2019; Zhu et al. 2013). Nonlegacy PCBs, also called unintentionally produced PCBs, now represent the major source of PCBs in the atmosphere of China (Zhao et al. 2020).

Lower-chlorinated PCBs, including PCBs 3, 11, and 52, are susceptible to cytochrome P450 enzyme-catalyzed biotransformation that was reviewed elsewhere (Grimm et al. 2015a; Liu et al. 2011, 2009; Matthews and Kato 1979; Safe et al. 1985). Chemical synthesis of authentic standards for hydroxylated and sulfated metabolites of PCBs 3, 11, and 52 allowed for inclusion of the individual PCB metabolites in the *in vitro* testing and thus reconstruction of major metabolic pathways at the individual congener level to evaluate bioactivation potential associated with lower-chlorinated PCBs (Lehmler and Robertson 2001; Li et al. 2010). Higher-chlorinated PCBs included both coplanar, dioxin-like PCB 126, and ortho-substituted, noncoplanar congeners (PCBs 95, 136, and 153). Penta-chlorinated PCB 95 was specifically selected for its known ability to act as a stimulant capable of sensitizing cellular calcium release through a mechanism involving interactions with the ryanodine receptor (RyR) (Wong et al. 2001, 1997; Wong and Pessah 1997). The RyR is a known regulator of cardiac Ca^{2+} homeostasis and was implicated in cardiovascular disease states such as arrhythmias (Pessah et al. 2010).

We chose to focus our *in vitro* studies on the potential of these substances to affect CMs and ECs, cells from tissues that are not traditionally included in acute, subchronic, or chronic rodent toxicity studies. Evidence that PCBs may have cardiovascular effects has been found. A recent cohort study evaluating dietary PCB exposure in approximately 70,000 individuals in Sweden revealed an increased risk of heart failure (Åkesson et al. 2019). These findings were concordant with previous observations correlating dietary PCB exposure with the development of hypertension in overweight subjects (Raffetti et al. 2018) and increased risk of myocardial infarction in men (Bergkvist et al. 2016). Follow-up studies of the health of the highly exposed Yusho and YuCheng cohorts, revealed that heart disease risk was increased over that of age- and sex-matched controls (Akahane et al. 2018; Li et al. 2015). Mechanistic evidence for population-based observations stems from both *in vitro* and *in vivo* studies examining the cardiovascular effects of individual PCB congeners and mixtures. Cardiovascular toxicity in zebrafish, including pericardial edema, cardiac looping defects, and circulatory failure have been reported upon exposure to PCB 126 and Aroclor 1254 (Li et al. 2014; Teixidó et al. 2019).

A number of *in vitro* studies have indicated multiple mechanisms for vascular damage elicited by PCBs (Hennig et al. 2002, 2005). PCBs 77, 114, 118, and 126, all aryl hydrocarbon receptor (AhR) agonists, are potent inducers of EC toxicity. Effects observed in porcine pulmonary artery–derived EC included disrupted endothelial barrier function, increased oxidative stress, and alteration in intracellular calcium levels (Toborek et al. 1995). Other studies have confirmed these changes and also reported inflammatory responses and apoptosis (Liu et al. 2015; Tang et al. 2017; Wahlang et al. 2016). Higher chlorinated biphenyls like PCB 153 were much less potent in most of these studies. Because only a few studies of endothelial toxicity have examined the lower chlorinated biphenyls or their metabolites, the current study represented an important advance in our knowledge.

There is also paucity of data on the potential cardiomyocyte effects of PCBs. The direct action of PCBs 19, 77, and 126, and the PCB mixture Aroclor 1254 on CMs from selected avian and rodent species has been investigated. PCBs' alteration of intracellular Ca^{2+} dynamics (Rebuzzini et al. 2018) and cardiac electrophysiology (Park et al. 2012) have been reported, in addition to the potential role of microRNAs in mediating the effects of PCBs during the differentiation of P19 cells into CMs (Zhu et al. 2012).

Our results clearly showed that PCBs and their metabolites were bioactive in both ECs and CMs, providing empirical evidence for their potential cardiovascular hazards. We also found structure– and metabolite class–specific trends in aggregate bioactivity indicated by ToxPi scores, suggesting that these effects are broadly applicable across the range of PCBs and their metabolites. To characterize the potential risk given current exposures, we compared our *in vitro* PODs with serum levels from recent biomonitoring studies. One limitation was that many more PCBs and metabolites have been detected than have been tested, so we demonstrated the use of read-across approaches to fill this data gap. Under "conservative" read-across, where data gaps are filled with "high-end" estimates, the most MOEs were less than 100 for CMs and less than 10 for ECs. Thus, although effective

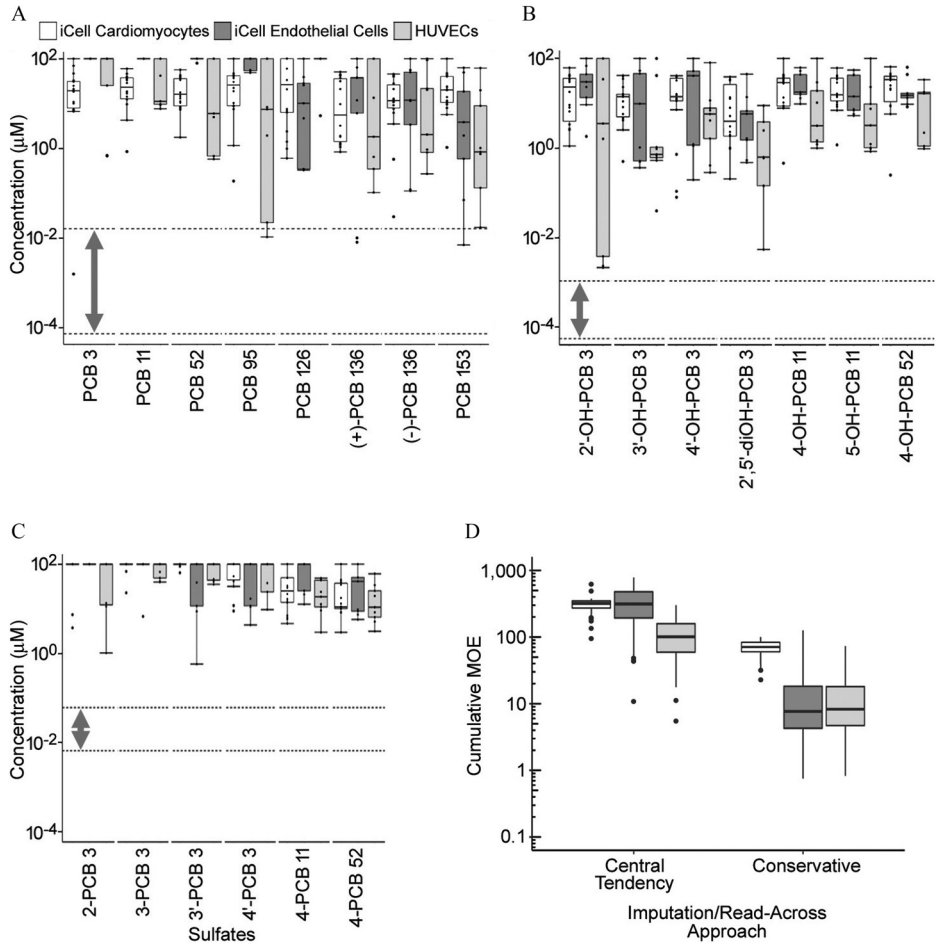

Figure 7. Characterization of the margins of exposure for (A) PCBs, (B) OH-PCBs, and (C) PCB sulfates separately, as well as for the cumulative effect all serum PCBs and metabolites together using an imputation/read-across approach (D). In (A–C), box plots show distributions of point-of-departure values (one standard deviation of the variability in cells treated with vehicle) for various phenotypes sorted by cell type (white: iCell®-cardiomyocytes; dark gray: iCell®-endothelial cells; light gray: human umbilical vein ECs (HUVECs). Dotted lines with bidirectional arrows are indicative of human serum concentration ranges for selected PCBs, OHPCBs, and PCB sulfates. In (D), box plots show the distribution across individuals in the biomonitoring studies (Ampleman et al. 2015; Grimm et al. 2017; Koh et al. 2016a, 2016b), of their cumulative margin of exposure across all PCBs and metabolites. Each cell type is cumulated separately, and both a "central tendency" and a "conservative" imputation/read across approach are used. All box plots were generated in ggplot2 R package (version 3.1; R Development Core Team) and indicate 25th, 50th (median), and 75th percentiles. Whiskers indicate the smallest and largest values within 1.5 × interquartile range above the 75th or below the 25th percentile. Outliers are indicated as dots. Chemical names and abbreviations of PCBs and metabolites are listed in Table S1. Note: CMs, cardiomyocytes; ECs, endothelial cells; HUVECs, human umbilical vein endothelial cells; OHPCBs, hydroxylated metabolites of PCBs; PCBs, polychlorinated biphenyls.

concentrations exceeded the levels measured in the general population, risks cannot entirely be ruled out due to the potential for population variability in susceptibility. The MOEs were comfortable under "central tendency" read-across, thus showing the need to fill these data gaps to make more confident statements about potential risks. The large amount of "missing data" on bioactivity, in addition to the relatively small MOEs under conservative read-across assumptions, suggested that either additional data collection or improved read-across approaches, such as applying quantitative structure–activity relationship (QSAR), may be necessary to reduce uncertainty and refine estimates for the cumulative risks from PCBs and metabolites. Alternatively, testing of whole mixtures of PCB congeners and metabolites may be useful to more directly characterize cumulative risks.

Although the data presented herein advance our knowledge of the structure–activity relationships in PCBs' and their metabolites' effects on CMs and ECs, there were a number of limitations. First, these *in vitro* studies examined only acute cardiotoxic and vascular effects of PCBs and PCB metabolites. Although this study design was consistent with accidental poisoning with PCB in spill scenarios, it did not address long-term exposures to PCBs in the general population. Adaptation of the experimental design to longer duration studies is therefore a recommended path forward. In addition, the cell models we used, iPSC-CMs, ECs, and HUVEC, and the phenotypes that were collected, captured only some of the potential chemically induced cardiovascular effects. Contractile force, cardiomyopathy, and other *in vivo* disease states may require additional experiments and different approaches. In this respect, the use of the microphysiological systems for both heart (Mathur et al. 2015) and the vasculature (Sobrino et al. 2016) promises to narrow this gap and offer enhanced physiological relevance.

Overall, we have demonstrated the importance and impact of characterizing cardiovascular-related bioactivity of not only parent PCBs but also their metabolites to have a more complete picture of potential cardiovascular risks. Our results provided additional biological plausibility to the association between PCB exposure and cardiovascular effects and suggest that such effects are common across this class of compounds. An important aspect is that we identified structural moieties associated with cardiovascular activity, including chlorination and metabolic status, and established biological similarity for closely related compounds. Oxidation appeared to play a key role in the bioactivation of PCBs to enhanced

cardiovascular active metabolites, whereas conjugation yielding PCB methoxylates and sulfates resulted in decreased biological activity. In a similar manner, there was a trend across the PCBs that indicated an association between increased chlorination and increased *in vitro* cardiovascular activity. The knowledge and conceptual trends identified in this study may have implications for related classes of halogenated chemicals, including polybrominated diphenyl ethers (PBDEs) (Gump et al. 2014; Jing et al. 2019), and dioxins (Humblet et al. 2008). Evaluating cumulative effects of PCBs and their metabolites requires estimates of potency across all PCBs and metabolites, which may be difficult to obtain experimentally. Because there appeared to be some relationship between structure and potency, either read-across and/or QSAR modeling are reasonable approaches to consider in filling these data gaps. The use of read-across with conservative assumptions suggests that for some individuals, the MOEs may be less than 10 or even near 1, given current exposures as indicated by biomonitoring data. This study thus demonstrated not only a strategy for incorporation of metabolite screening into *in vitro* testing, but also showed how these approaches can be implemented to characterize human health risks from complex mixtures of PCBs and their metabolites.

Acknowledgments

The authors wish to thank P. Thorne (University of Iowa) for providing human exposure data. This work was supported, in part, by grants from the National Institutes of Health (NIH) (P42 ES027704, P30 ES029067, and P42 ES013661) and a cooperative agreement with the United States Environmental Protection Agency (STAR RD83580201). The views expressed in this manuscript do not reflect those of the funding agencies. The use of specific commercial products in this work does not constitute endorsement by the funding agencies. W.D.K. was supported by NIH T32 ES026568.

References

Akahane M, Matsumoto S, Kanagawa Y, Mitoma C, Uchi H, Yoshimura T, et al. 2018. Long-term health effects of PCBs and related compounds: a comparative analysis of patients suffering from Yusho and the general population. Arch Environ Contam Toxicol 74(2):203–217, PMID: 29256109, https://doi.org/10.1007/s00244-017-0486-6.

Åkesson A, Donat-Vargas C, Berglund M, Glynn A, Wolk A, Kippler M. 2019. Dietary exposure to polychlorinated biphenyls and risk of heart failure–a population-based prospective cohort study. Environ Int 126:1–6, PMID: 30776745, https://doi.org/10.1016/j.envint.2019.01.069.

Amaro AR, Oakley GG, Bauer U, Spielmann HP, Robertson LW. 1996. Metabolic activation of PCBs to quinones: reactivity toward nitrogen and sulfur nucleophiles and influence of superoxide dismutase. Chem Res Toxicol 9(3):623–629, PMID: 8728508, https://doi.org/10.1021/tx950117e.

Ampleman MD, Martinez A, DeWall J, Rawn DF, Hornbuckle KC, Thorne PS. 2015. Inhalation and dietary exposure to PCBs in urban and rural cohorts via congener-specific measurements. Environ Sci Technol 49(2):1156–1164, PMID: 25510359, https://doi.org/10.1021/es5048039.

Arulmozhiraja S, Shiraishi F, Okumura T, Iida M, Takigami H, Edmonds JS, et al. 2005. Structural requirements for the interaction of 91 hydroxylated polychlorinated biphenyls with estrogen and thyroid hormone receptors. Toxicol Sci 84(1):49–62, PMID: 15601674, https://doi.org/10.1093/toxsci/kfi063.

Bauer U, Amaro AR, Robertson LW. 1995. A new strategy for the synthesis of polychlorinated biphenyl metabolites. Chem Res Toxicol 8(1):92–95, PMID: 7703372, https://doi.org/10.1021/tx00043a012.

Bergkvist C, Berglund M, Glynn A, Julin B, Wolk A, Åkesson A. 2016. Dietary exposure to polychlorinated biphenyls and risk of myocardial infarction in men–a population-based prospective cohort study. Environ Int 88:9–14, PMID: 26690540, https://doi.org/10.1016/j.envint.2015.11.020.

Blanchette AD, Grimm FA, Dalaijamts C, Hsieh NH, Ferguson K, Luo YS, et al. 2019. Thorough QT/QTc in a dish: an in vitro human model that accurately predicts clinical concentration-QTc relationships. Clin Pharmacol Ther 105(5):1175–1186, PMID: 30346629, https://doi.org/10.1002/cpt.1259.

Bolgar M, Cunningham J, Cooper R, Kozloski R, Hubball J, Miller DP, et al. 1995. Physical, spectral and chromatographic properties of all 209 individual PCB congeners. Chemosphere 31(2):2687–2705, https://doi.org/10.1016/0045-6535(95)00140-4.

Burnett SD, Blanchette AD, Grimm FA, House JS, Reif DM, Wright FA, et al. 2019. Population-based toxicity screening in human induced pluripotent stem cell-derived cardiomyocytes. Toxicol Appl Pharmacol 381:114711, PMID: 31425687, https://doi.org/10.1016/j.taap.2019.114711.

Combes RD. 2011. Challenges for computational structure-activity modelling for predicting chemical toxicity: future improvements? Expert Opin Drug Metab Toxicol 7(9):1129–1140, PMID: 21756202, https://doi.org/10.1517/17425255.2011.602066.

Cronin MTD, Enoch SJ, Mellor CL, Przybylak KR, Richarz AN, Madden JC. 2017. In silico prediction of organ level toxicity: linking chemistry to adverse effects. Toxicol Res 33(3):173–182, PMID: 28744348, https://doi.org/10.5487/TR.2017.33.3.173.

Dimitrov SD, Diderich R, Sobanski T, Pavlov TS, Chankov GV, Chapkanov AS, et al. 2016. QSAR Toolbox–workflow and major functionalities. SAR QSAR Environ Res 27(3): 1–17, PMID: 26892800, https://doi.org/10.1080/1062936X.2015.1136680.

Grimm FA, Blanchette A, House JS, Ferguson K, Hsieh NH, Dalaijamts C, et al. 2018. A human population-based organotypic in vitro model for cardiotoxicity screening. ALTEX 35(4):441–452, PMID: 29999168, https://doi.org/10.14573/altex.1805301.

Grimm FA, Hu D, Kania-Korwel I, Lehmler HJ, Ludewig G, Hornbuckle KC, et al. 2015a. Metabolism and metabolites of polychlorinated biphenyls. Crit Rev Toxicol 45(3):245–272, PMID: 25629923, https://doi.org/10.3109/10408444.2014.999365.

Grimm FA, Iwata Y, Sirenko O, Bittner M, Rusyn I. 2015b. High-content assay multiplexing for toxicity screening in induced pluripotent stem cell-derived cardiomyocytes and hepatocytes. Assay Drug Dev Technol 13(9):529–546, PMID: 26539751, https://doi.org/10.1089/adt.2015.659.

Grimm FA, Lehmler HJ, Koh WX, DeWall J, Teesch LM, Hornbuckle KC, et al. 2017. Identification of a sulfate metabolite of PCB 11 in human serum. Environ Int 98:120–128, PMID: 27816204, https://doi.org/10.1016/j.envint.2016.10.023.

Gump BB, Yun S, Kannan K. 2014. Polybrominated diphenyl ether (PBDE) exposure in children: possible associations with cardiovascular and psychological functions. Environ Res 132:244–250, PMID: 24834818, https://doi.org/10.1016/j.envres.2014.04.009.

Haws LC, Su SH, Harris M, Devito MJ, Walker NJ, Farland WH, et al. 2006. Development of a refined database of mammalian relative potency estimates for dioxin-like compounds. Toxicol Sci 89(1):4–30, PMID: 16120753, https://doi.org/10.1093/toxsci/kfi294.

Hennig B, Hammock BD, Slim R, Toborek M, Saraswathi V, Robertson LW. 2002. PCB-induced oxidative stress in endothelial cells: modulation by nutrients. Int J Hyg Environ Health 205(1–2):95–102, PMID: 12018021, https://doi.org/10.1078/1438-4639-00134.

Hennig B, Reiterer G, Majkova Z, Oesterling E, Meerarani P, Toborek M. 2005. Modification of environmental toxicity by nutrients: implications in atherosclerosis. Cardiovasc Toxicol 5(2):153–160, PMID: 16046791, https://doi.org/10.1385/ct:5:2:153.

Herrick RF, Stewart JH, Allen JG. 2016. Review of PCBs in US schools: a brief history, an estimate of the number of impacted schools, and an approach for evaluating indoor air samples. Environ Sci Pollut Res Int 23(3):1975–1985, PMID: 25940477, https://doi.org/10.1007/s11356-015-4574-8.

Holland EB, Feng W, Zheng J, Dong Y, Li X, Lehmler HJ, et al. 2017. An extended structure-activity relationship of nondioxin-like PCBs evaluates and supports modeling predictions and identifies picomolar potency of PCB 202 towards ryanodine receptors. Toxicol Sci 155(1):170–181, PMID: 27655348, https://doi.org/10.1093/toxsci/kfw189.

Hu D, Hornbuckle KC. 2010. Inadvertent polychlorinated biphenyls in commercial paint pigments. Environ Sci Technol 44(8):2822–2827, PMID: 19957996, https://doi.org/10.1021/es902413k.

Humblet O, Birnbaum L, Rimm E, Mittleman MA, Hauser R. 2008. Dioxins and cardiovascular disease mortality. Environ Health Perspect 116(11):1443–1448, PMID: 19057694, https://doi.org/10.1289/ehp.11579.

Iwata Y, Klaren WD, Lebakken CS, Grimm FA, Rusyn I. 2017. High-content assay multiplexing for vascular toxicity screening in induced pluripotent stem cell-derived endothelial cells and human umbilical vein endothelial cells. Assay Drug Dev Technol 15(6):267–279, PMID: 28771372, https://doi.org/10.1089/adt.2017.786.

Jing L, Sun Y, Wang Y, Liang B, Chen T, Zheng D, et al. 2019. Cardiovascular toxicity of decabrominated diphenyl ethers (BDE-209) and decabromodiphenyl ethane (DBDPE) in rats. Chemosphere 223:675–685, PMID: 30802833, https://doi.org/10.1016/j.chemosphere.2019.02.115.

Joshi SN, Vyas SM, Duffel MW, Parkin S, Lehmler HJ. 2011. Synthesis of sterically hindered polychlorinated biphenyl derivatives. Synthesis (Stuttg) 7:1045–1054, PMID: 21516177, https://doi.org/10.1055/s-0030-1258454.

Kania-Korwel I, Hrycay EG, Bandiera SM, Lehmler HJ. 2008. 2,2′,3,3′,6,6′-Hexachlorobiphenyl (PCB 136) atropisomers interact enantioselectively with hepatic microsomal cytochrome P450 enzymes. Chem Res Toxicol 21(6):1295–1303, PMID: 18494506, https://doi.org/10.1021/tx800059j.

Kavlock RJ, Bahadori T, Barton-Maclaren TS, Gwinn MR, Rasenberg M, Thomas RS. 2018. Accelerating the pace of chemical risk assessment. Chem Res Toxicol 31(5):287–290, PMID: 29600706, https://doi.org/10.1021/acs.chemrestox.7b00339.

Kitamura S, Jinno N, Suzuki T, Sugihara K, Ohta S, Kuroki H, et al. 2005. Thyroid hormone-like and estrogenic activity of hydroxylated PCBs in cell culture. Toxicology 208(3):377–387, PMID: 15695023, https://doi.org/10.1016/j.tox.2004.11.037.

Koh WX, Hornbuckle KC, Marek RF, Wang K, Thorne PS. 2016a. Hydroxylated polychlorinated biphenyls in human sera from adolescents and their mothers living in two U.S. midwestern communities. Chemosphere 147:389–395, PMID: 26774304, https://doi.org/10.1016/j.chemosphere.2015.12.113.

Koh WX, Hornbuckle KC, Wang K, Thorne PS. 2016b. Serum polychlorinated biphenyls and their hydroxylated metabolites are associated with demographic and behavioral factors in children and mothers. Environ Int 94:538–545, PMID: 27352881, https://doi.org/10.1016/j.envint.2016.06.014.

Lallas PL. 2001. The Stockholm Convention on Persistent Organic Pollutants. Am J Int Law 95(3):692–708, https://doi.org/10.2307/2668517.

Lauby-Secretan B, Loomis D, Baan R, El Ghissassi F, Bouvard V, Benbrahim-Tallaa L, et al. 2016. Use of mechanistic data in the IARC evaluations of the carcinogenicity of polychlorinated biphenyls and related compounds. Environ Sci Pollut Res Int 23(3):2220–2229, PMID: 26077316, https://doi.org/10.1007/s11356-015-4829-4.

Lauby-Secretan B, Loomis D, Grosse Y, El Ghissassi F, Bouvard V, Benbrahim-Tallaa L, et al. 2013. Carcinogenicity of polychlorinated biphenyls and polybrominated biphenyls. Lancet Oncol 14(4):287–288, PMID: 23499544, https://doi.org/10.1016/S1470-2045(13)70104-9.

Lehmler HJ, Robertson LW. 2001. Synthesis of hydroxylated PCB metabolites with the Suzuki-coupling. Chemosphere 45(8):1119–1127, PMID: 11695625, https://doi.org/10.1016/s0045-6535(01)00052-2.

Li MC, Chen PC, Tsai PC, Furue M, Onozuka D, Hagihara A, et al. 2015. Mortality after exposure to polychlorinated biphenyls and polychlorinated dibenzofurans: a meta-analysis of two highly exposed cohorts. Int J Cancer 137(6):1427–1432, PMID: 25754105, https://doi.org/10.1002/ijc.29504.

Li X, Holland EB, Feng W, Zheng J, Dong Y, Pessah IN, et al. 2018. Authentication of synthetic environmental contaminants and their (bio)transformation products in toxicology: polychlorinated biphenyls as an example. Environ Sci Pollut Res Int 25(17):16508–16521, PMID: 29322390, https://doi.org/10.1007/s11356-017-1162-0.

Li X, Parkin S, Duffel MW, Robertson LW, Lehmler HJ. 2010. An efficient approach to sulfate metabolites of polychlorinated biphenyls. Environ Int 36(8):843–848, PMID: 19345419, https://doi.org/10.1016/j.envint.2009.02.005.

Li M, Wang X, Zhu J, Zhu S, Hu X, Zhu C, et al. 2014. Toxic effects of polychlorinated biphenyls on cardiac development in zebrafish. Mol Biol Rep 41(12):7973–7983, PMID: 25163633, https://doi.org/10.1007/s11033-014-3692-6.

Liu Y, Lehmler HJ, Robertson LW, Duffel MW. 2011. Physicochemical properties of hydroxylated polychlorinated biphenyls aid in predicting their interactions with rat sulfotransferase 1A1 (rSULT1A1). Chem Biol Interact 189(3):153–160, PMID: 21130751, https://doi.org/10.1016/j.cbi.2010.11.009.

Liu D, Perkins JT, Petriello MC, Hennig B. 2015. Exposure to coplanar PCBs induces endothelial cell inflammation through epigenetic regulation of NF-κB subunit p65. Toxicol Appl Pharmacol 289(3):457–465, PMID: 26519613, https://doi.org/10.1016/j.taap.2015.10.015.

Liu Y, Smart JT, Song Y, Lehmler HJ, Robertson LW, Duffel MW. 2009. Structure-activity relationships for hydroxylated polychlorinated biphenyls as substrates and inhibitors of rat sulfotransferases and modification of these relationships by changes in thiol status. Drug Metab Dispos 37(5):1065–1072, PMID: 19196841, https://doi.org/10.1124/dmd.108.026021.

Low Y, Sedykh A, Fourches D, Golbraikh A, Whelan M, Rusyn I, et al. 2013. Integrative chemical-biological read-across approach for chemical hazard classification. Chem Res Toxicol 26(8):1199–1208, PMID: 23848138, https://doi.org/10.1021/tx400110f.

Ludewig G, Robertson LW. 2013. Polychlorinated biphenyls (PCBs) as initiating agents in hepatocellular carcinoma. Cancer Lett 334(1):46–55, PMID: 23211541, https://doi.org/10.1016/j.canlet.2012.11.041.

Marek RF, Thorne PS, Herkert NJ, Awad AM, Hornbuckle KC. 2017. Airborne PCBs and OH-PCBs inside and outside urban and rural U.S. schools. Environ Sci Technol 51(14):7853–7860, PMID: 28656752, https://doi.org/10.1021/acs.est.7b01910.

Marvel SW, To K, Grimm FA, Wright FA, Rusyn I, Reif DM. 2018. ToxPi Graphical User Interface 2.0: dynamic exploration, visualization, and sharing of integrated data models. BMC Bioinformatics 19(1):80, PMID: 29506467, https://doi.org/10.1186/s12859-018-2089-2.

Mathews HB, Anderson MW. 1975. Effect of chlorination on the distribution and excretion of polychlorinated biphenyls. Drug Metab Dispos 3(5):371–380, PMID: 241618.

Mathur A, Loskill P, Shao K, Huebsch N, Hong S, Marcus SG, et al. 2015. Human iPSC-based cardiac microphysiological system for drug screening applications. Sci Rep 5:8883, PMID: 25748532, https://doi.org/10.1038/srep08883.

Matthews HB, Kato S. 1979. The metabolism and disposition of halogenated aromatics. Ann NY Acad Sci 320:131–137, PMID: 110188, https://doi.org/10.1111/j.1749-6632.1979.tb56596.x.

McLean MR, Bauer U, Amaro AR, Robertson LW. 1996. Identification of catechol and hydroquinone metabolites of 4-monochlorobiphenyl. Chem Res Toxicol 9(1):158–164, PMID: 8924585, https://doi.org/10.1021/tx950083a.

Mekenyan O, Dimitrov S, Pavlov T, Dimitrova G, Todorov M, Petkov P, et al. 2012. Simulation of chemical metabolism for fate and hazard assessment. v. mammalian hazard assessment. SAR QSAR Environ Res 23(5–6):553–606, PMID: 22536822, https://doi.org/10.1080/1062936X.2012.679689.

Mills RA, Millis CD, Dannan GA, Guengerich FP, Aust SD. 1985. Studies on the structure-activity relationships for the metabolism of polybrominated biphenyls by rat liver microsomes. Toxicol Appl Pharmacol 78(1):96–104, PMID: 2994255, https://doi.org/10.1016/0041-008X(85)90309-6.

Park MH, Park WS, Jo SH. 2012. Acute alteration of cardiac ECG, action potential, I (Kr) and the human ether-a-go-go-related gene (hERG) K+ channel by PCB 126 and PCB 77. Toxicol Appl Pharmacol 262(1):60–69, PMID: 22676973, https://doi.org/10.1016/j.taap.2012.04.019.

Paul Friedman K, Gagne M, Loo LH, Karamertzanis P, Netzeva T, Sobanski T, et al. 2020. Utility of in vitro bioactivity as a lower bound estimate of in vivo adverse effect levels and in risk-based prioritization. Toxicol Sci 173(1):202–225, PMID: 31532525, https://doi.org/10.1093/toxsci/kfz201.

Pessah IN, Cherednichenko G, Lein PJ. 2010. Minding the calcium store: ryanodine receptor activation as a convergent mechanism of PCB toxicity. Pharmacol Ther 125(2):260–285, PMID: 19931307, https://doi.org/10.1016/j.pharmthera.2009.10.009.

Raffetti E, Donato F, Speziani F, Scarcella C, Gaia A, Magoni M. 2018. Polychlorinated biphenyls (PCBs) exposure and cardiovascular, endocrine and metabolic diseases: a population-based cohort study in a North Italian highly polluted area. Environ Int 120:215–222, PMID: 30103120, https://doi.org/10.1016/j.envint.2018.08.022.

Rebuzzini P, Zuccolo E, Civello C, Fassina L, Arechaga J, Izquierdo A, et al. 2018. Polychlorinated biphenyls reduce the kinematics contractile properties of embryonic stem cells-derived cardiomyocytes by disrupting their intracellular Ca^{2+} dynamics. Sci Rep 8(1):17909, PMID: 30559452, https://doi.org/10.1038/s41598-018-36333-z.

Rodrigues RM, Bouhifd M, Bories G, Sacco MG, Gribaldo L, Fabbri M, et al. 2013. Assessment of an automated in vitro basal cytotoxicity test system based on metabolically-competent cells. Toxicol In Vitro 27(2):760–767, PMID: 23261643, https://doi.org/10.1016/j.tiv.2012.12.004.

Safe S. 1993. Toxicology, structure-function relationship, and human and environmental health impacts of polychlorinated biphenyls: progress and problems. Environ Health Perspect 100:259–268, PMID: 8354174, https://doi.org/10.1289/ehp.93100259.

Safe S, Bandiera S, Sawyer T, Robertson L, Safe L, Parkinson A, et al. 1985. PCBs: structure–function relationships and mechanism of action. Environ Health Perspect 60:47–56, PMID: 2992927, https://doi.org/10.1289/ehp.856047.

Sethi S, Keil KP, Chen H, Hayakawa K, Li X, Lin Y, et al. 2017. Detection of 3,3′-dichlorobiphenyl in human maternal plasma and its effects on axonal and dendritic growth in primary rat neurons. Toxicol Sci 158(2):401–411, PMID: 28510766, https://doi.org/10.1093/toxsci/kfx100.

Sethi S, Morgan RK, Feng W, Lin Y, Li X, Luna C, et al. 2019. Comparative analyses of the 12 most abundant PCB congeners detected in human maternal serum for activity at the thyroid hormone receptor and ryanodine receptor. Environ Sci Technol 53(7):3948–3958, PMID: 30821444, https://doi.org/10.1021/acs.est.9b00535.

Shaikh NS, Parkin S, Lehmler HJ. 2006. The Ullmann Coupling Reaction: a new approach to tetraarylstannanes. Organometallics 25(17):4207–4214, https://doi.org/10.1021/om060456a.

Silberhorn EM, Glauert HP, Robertson LW. 1990. Carcinogenicity of polyhalogenated biphenyls: PCBs and PBBs. Crit Rev Toxicol 20(6):440–496, PMID: 2165409, https://doi.org/10.3109/10408449009029331.

Sirenko O, Crittenden C, Callamaras N, Hesley J, Chen YW, Funes C, et al. 2013a. Multiparameter in vitro assessment of compound effects on cardiomyocyte physiology using iPSC cells. J Biomol Screen 18(1):39–53, PMID: 22972846, https://doi.org/10.1177/1087057112457590.

Sirenko O, Cromwell EF, Crittenden C, Wignall JA, Wright FA, Rusyn I. 2013b. Assessment of beating parameters in human induced pluripotent stem cells enables quantitative in vitro screening for cardiotoxicity. Toxicol Appl Pharmacol 273(3):500–507, PMID: 24095675, https://doi.org/10.1016/j.taap.2013.09.017.

Sirenko O, Grimm FA, Ryan KR, Iwata Y, Chiu WA, Parham F, et al. 2017. In vitro cardiotoxicity assessment of environmental chemicals using an organotypic human induced pluripotent stem cell-derived model. Toxicol Appl Pharmacol 322:60–74, PMID: 28259702, https://doi.org/10.1016/j.taap.2017.02.020.

Sobrino A, Phan DT, Datta R, Wang X, Hachey SJ, Romero-López M, et al. 2016. 3D microtumors in vitro supported by perfused vascular networks. Sci Rep 6:31589, PMID: 27549930, https://doi.org/10.1038/srep31589.

Tang L, Cheng JN, Long Y, He XM, Liang GN, Tang XP, et al. 2017. PCB 118-induced endothelial cell apoptosis is partially mediated by excessive ROS production. Toxicol Mech Methods 27(5):394–399, PMID: 28399781, https://doi.org/10.1080/15376516.2017.1296050.

Teixidó E, Barenys M, Piqué E, Llobet JM, Gomez-Catalán J. 2019. Cardiovascular effects of PCB 126 (3,3′,4,4′,5-Pentachlorobiphenyl) in zebrafish embryos and impact of co-exposure to redox modulating chemicals. Int J Mol Sci 20(5):1065, https://doi.org/10.3390/ijms20051065.

Toborek M, Barger SW, Mattson MP, Espandiari P, Robertson LW, Hennig B. 1995. Exposure to polychlorinated biphenyls causes endothelial cell dysfunction. J Biochem Toxicol 10(4):219–226, PMID: 8568836, https://doi.org/10.1002/jbt.2570100406.

U.S. EPA (U.S. Environmental Protection Agency). 2012. Benchmark Dose Technical Guidance. Washington, DC: Risk Assessment Forum, U.S. Environmental Protection Agency.

U.S. EPA. 2005. Guidelines for Carcinogen Risk Assessment. Washington, DC: Risk Assessment Forum, U.S. Environmental Protection Agency.

U.S. EPA. 2003. Table of PCB Species by Congener Number. Washington, DC: U.S. Environmental Protection Agency.

U.S. FDA (U.S. Food and Drug Administration). 2017. In Vitro Metabolism- and Transporter-Mediated Drug-Drug Interaction Studies: Guidance for Industry (Draft Guidance). Silver Spring, MD: U.S. Food and Drug Administration.

Van den Berg M, Birnbaum LS, Denison M, De Vito M, Farland W, Feeley M, et al. 2006. The 2005 World Health Organization reevaluation of human and mammalian toxic equivalency factors for dioxins and dioxin-like compounds. Toxicol Sci 93(2):223–241, PMID: 16829543, https://doi.org/10.1093/toxsci/kfl055.

van der Voet H, van der Heijden GW, Bos PM, Bosgra S, Boon PE, Muri SD, et al. 2009. A model for probabilistic health impact assessment of exposure to food chemicals. Food Chem Toxicol 47(12):2926–2940, PMID: 19150381, https://doi.org/10.1016/j.fct.2008.12.027.

van Ede KI, van Duursen MB, van den Berg M. 2016. Evaluation of relative effect potencies (REPs) for dioxin-like compounds to derive systemic or human-specific TEFs to improve human risk assessment. Arch Toxicol 90(6):1293–1305, PMID: 27161441, https://doi.org/10.1007/s00204-016-1724-9.

Wahlang B, Petriello MC, Perkins JT, Shen S, Hennig B. 2016. Polychlorinated biphenyl exposure alters the expression profile of microRNAs associated with vascular diseases. Toxicol in Vitro 35:180–187, PMID: 27288564, https://doi.org/10.1016/j.tiv.2016.06.001.

Wong PW, Garcia EF, Pessah IN. 2001. *ortho*-substituted PCB95 alters intracellular calcium signaling and causes cellular acidification in PC12 cells by an immunophilin-dependent mechanism. J Neurochem 76(2):450–463, PMID: 11208908, https://doi.org/10.1046/j.1471-4159.2001.00022.x.

Wong PW, Joy RM, Albertson TE, Schantz SL, Pessah IN. 1997. Ortho-substituted 2,2′,3,5′,6-pentachlorobiphenyl (PCB 95) alters rat hippocampal ryanodine receptors and neuroplasticity in vitro: evidence for altered hippocampal function. Neurotoxicology 18(2):443–456, PMID: 9291493.

Wong PW, Pessah IN. 1997. Noncoplanar PCB 95 alters microsomal calcium transport by an immunophilin FKBP12-dependent mechanism. Mol Pharmacol 51(5):693–702, PMID: 9145907, https://doi.org/10.1124/mol.51.5.693.

Zhao S, Jones KC, Li J, Sweetman AJ, Liu X, Xu Y, et al. 2020. Evidence for major contributions of unintentionally produced PCBs in the air of China: implications for the National Source Inventory. Environ Sci Technol 54(4):2163–2171, PMID: 31851493, https://doi.org/10.1021/acs.est.9b06051.

Zhu Y, Mapuskar KA, Marek RF, Xu W, Lehmler HJ, Robertson LW, et al. 2013. A new player in environmentally induced oxidative stress: polychlorinated biphenyl congener, 3,3′-dichlorobiphenyl (PCB11). Toxicol Sci 136(1):39–50, PMID: 23997111, https://doi.org/10.1093/toxsci/kft186.

Zhu C, Yu ZB, Zhu JG, Hu XS, Chen YL, Qiu YF, et al. 2012. Differential expression profile of MicroRNAs during differentiation of cardiomyocytes exposed to polychlorinated biphenyls. Int J Mol Sci 13(12):15955–15966, PMID: 23443104, https://doi.org/10.3390/ijms131215955.